INTERNATIONAL ATOMIC ENERGY AGENCY
UNITED NATIONS EDUCATIONAL, SCIENTIFIC AND CULTURAL ORGANIZATION
INTERNATIONAL CENTRE FOR THEORETICAL PHYSICS
I.C.T.P., P.O. BOX 586, 34100 TRIESTE, ITALY, CABLE: CENTRATOM TRIESTE

H4.SMR/453-24

TRAINING COLLEGE ON PHYSICS AND CHARACTERIZATION OF LASERS AND OPTICAL FIBRES

(5 February - 2 March 1990)

A NUMERICAL INVESTIGATION ON A C.W. HIGH-POWER, ELECTRON-BEAM, PRE-IONIZED $He : N_2 : CO_2 : CO$ LASER†

S. Solimeno*
G. Mastrocinque*, L. Lanotte**
S. Martellucci & J. Quartieri****

***Istituto Elettrotecnico**
Facultà di Ingegneria
Università Napoli
80125 Napoli

****Istituto di Fisica dell Facoltà**
di Ingegneria, Università Napoli,

OPTICA ACTA, 1980, VOL. 27, NO. 8, 1275–1286

A numerical investigation on a c.w. high-power, electron-beam, pre-ionized $He : N_2 : CO_2 : CO$ laser†

G. MASTROCINQUE and S. SOLIMENO
Istituto Elettrotecnico, Facoltà di Ingegneria, Universitá Napoli, Italy

and L. LANOTTE, S. MARTELLUCCI and J. QUARTIERI
Istituto di Fisica della Facoltà di Ingegneria, Universitá Napoli, Italy

(*Received 16 July 1979*)

Abstract. We studied some kinetic, fluid-dynamic and electrical problems arising in the numerical modelling of a c.w. TE high power CO_2 laser operating with N_2, He and CO additives. We adapted a five-temperature pulsed laser model to the c.w. case by coupling a set of fluid-dynamic equations to the kinetic set. We added the rate equation for the secondary electron density. We calculated in some detail the ionization term and fitted experimental results to determine attachment and recombination coefficients in the discharge chamber. In order to solve our equations a numerical code has been developed. By this means we investigated the effects of temperature, density and velocity variations in the flowing mixture on the small signal gain of the device. We obtained profiles in the laser chamber of the sustainer current, small signal gain and fluid-dynamic parameters. A simple (Fabry–Perot) optical cavity model has been used to calculate output power and electrical efficiency of the device. A comparison of numerical code predictions and experimental results is presented.

1. Introduction

In a previous paper [1], some results obtained with a numerical algorithm predicting the performance of a c.w. TE high-power electron beam ionized CO_2 laser have been discussed. In that model, vibrational kinetic phenomena occurring in the laser channel were studied using a four-temperature set of equations. Fluid-dynamic effects were taken into account coupling the Euler's equations to the kinetic set via the enthalpy equation. Our calculations referred to a $He : N_2 : CO_2$ mixture. Profiles in the laser chamber of various quantities (electron density, fluid-dynamic parameters and small signal gain) were presented.

In this paper a few aspects of the proposed model are discussed in some detail, and theoretical results are compared with the available experimental data of an AVCO HPL 15 industrial laser. Since this device operates with a $He : N_2 : CO_2 : CO$ mixture we have extended the four-temperature kinetic model to a five-temperature one, including carbon monoxide.

The device investigated is shown schematically in figure 1. The discharge channel measures $10 \times 10 \times 150\ cm^3$ and contains two electrodes, usually of reticular or tubular type, either oil or water cooled. The electric discharge is directed according to the transverse horizontal dimension, and the gas flows along its vertical axis (y) downwards. Before entering the discharge chamber the laser mixture is

† Work partially sponsored by Centro Ricerche FIAT, Orbassano (TO), Italy.

0030-3909/80/2708 1275 $02.00/0

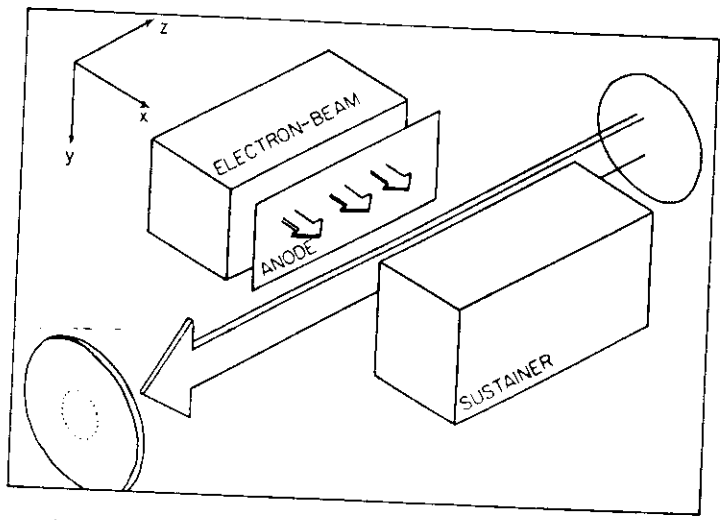

Figure 1. Geometry of the discharge chamber and of the optical cavity.

accelerated by a tapering conduit. The electron-beam pre-ionization device is mounted beside the discharge chamber. The beam of fast electrons ($E_{beam} \sim 70$ keV), referred to as the primary electrons, is generated in a high-vacuum enclosure. The latter is separated from the chamber containing the gas mixture by a thin metal foil (12·7 μm in thickness), generally of aluminium or titanium, which is traversed by the primary electrons. The foil is supported by a metal grid. At the ends of the chamber in the direction of the major axis there are three copper mirrors constituting the optical unstable resonator. The optical energy is extracted by means of a circular-ring mirror intercepting the outer skirts of the radiation beam returned by the concave reflector. The output beam, part of which goes back through the optically active region, is tilted slightly downwards and is concentrated onto an aerodynamic window.

The paper is organized as follows. In § 2 the electrical discharge and plasma characteristics which have been taken into account in the model are presented. In particular a method to estimate numerical values of some important parameters using experimental data is discussed. In § 3 the kinetic and fluid-dynamic set of equations is briefly recalled. In § 4 an outline of the small-signal gain and output optical power calculations is given. In § 5 the theoretical results are presented and compared with the available experimental data.

2. Electric discharge and plasma characteristics

In this section the secondary electron density N_e produced by the electron beam and the electrical power density W_{el} delivered to the medium are evaluated. One has:

$$W_{el} = J_s E = e N_e v_D E, \tag{1}$$

where e is the electron charge, J_s is the sustainer current density, E is the sustainer electric field and v_D is the electron drift velocity. Assuming local charge neutrality and a steady-state regime the equation for N_e reads:

$$v \frac{d}{dy} N_e = S - \alpha N_e^2 - \beta N_e, \tag{2}$$

where v is the gas flow velocity in the y direction, S is the number density of secondary electrons (source term) generated in the gas by the primary electron beam and α, β are the effective recombination and attachment coefficients of the mixture respectively. We are going now to assess numerical values for S, α, β.

2.1. *Source term*

Calculations of S are generally based on Bethe's formula for the ionization stopping power F of the medium or on modified later versions [2, 3]. Berger and Seltzer [4] have provided numerical calculations on the stopping power of various materials as a function of the primary electron energy. We have used the following equation:

$$S=\frac{J_b}{e}\sum_i \frac{X_i F_i}{E_{ion}^{(i)}}\equiv \varepsilon J_b, \tag{3}$$

where J_b is the electron beam current density, X_i and $E_{ion}^{(i)}$ are the volume fraction and mean ionization energy of the ith component of the mixture. F_i is the stopping power of the ith component as given by Rohrlich and Carlson [2]. By this means detailed calculations of primary electron energy and source term versus thickness of materials have been performed [5]. In particular, the energy loss experienced by a 70 keV incident electron beam across an Al foil has been determined, and a practically negligible variation of S along a 10 cm path in a typical laser mixture has been found. In table 1 some typical values of S for different mixtures and electron energies are reported from the last cited reference. The corresponding value for J_b is 0·03 mA/cm^2.

Table 1. Values of the source term S for some mixtures at 0·1 atm. U is the electron beam energy and S is expressed in 10^{15} cm^{-3} s^{-1}.

He:N_2:CO_2:CO	1000	0100	0010	0001	6411	3210	1010	3111
$U=70$ keV	0·339	3·17	5·10	3·17	1·92	2·08	2·72	2·08
$U=50$ keV	0·429	3·99	6·46	3·99	2·42	2·62	3·44	2·62
$U=30$ keV	0·639	5·91	9·49	5·91	3·57	3·87	5·06	3·87

2.2. *Recombination and attachment coefficients*

Values of α and β for high power lasers are difficult to assess. They depend critically on mixture impurities [6] and, even in the ideal case of a pure gas, their theoretical evaluation is extremely arduous. We have attempted to bypass this difficulty by using the operating characteristic I_s versus I_b—shown in figure 2 for a pressure of 0·1 atm—of the investigated device. In order to give an interpretation of the experimental figure we note that, assuming $S, \alpha, \beta, v \equiv S_0, \alpha_0, \beta_0, v_0 =$ constant in equation (2), one can perform integration of N_e over the discharge chamber cross-section. One obtains:

$$I_s = ev_{D_0}\int_0^{L_z} dz \int_0^{L_y} N_e(y)\,dy = \frac{2I_b}{\beta_0\varepsilon_0(1-R)} + \frac{4v_0 I_b}{L_y\beta_0^2\varepsilon_0(R^2-1)} \times \ln\frac{(R+1)\exp(\beta_0 R L_y/v_0)+R-1}{2R} \tag{4}$$

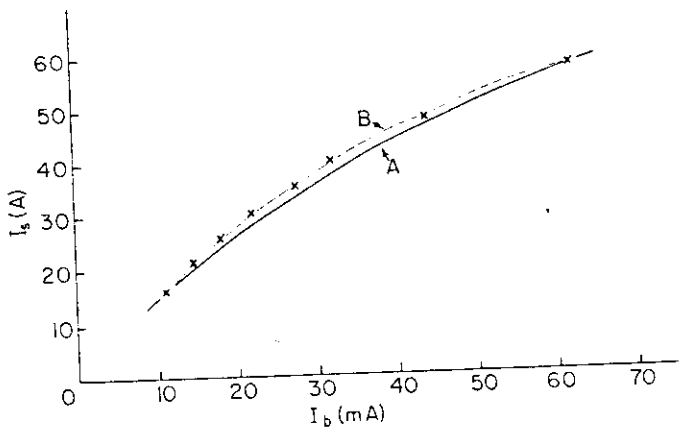

Figure 2. Sustainer current I_s versus electron beam current I_b: curve A, theoretical; curve B, experimental.

where I_s is the sustainer current, L_y and L_z are the appropriate discharge chamber dimensions, $I_b = J_b L_y L_z$ is the electron beam current, τ_{D_0} and ε_0 are the constant values used for τ_D, ε respectively and

$$R = \sqrt{\left(1 + \frac{4\alpha_0 \varepsilon_0 I_b}{\beta_0^2 L_y L_z}\right)} \equiv R(I_b) \tag{5}$$

is a parameter whose value depends on the relative importance of recombination with respect to attachment processes.

In the equation (4) the quantity $1/\beta_0 R = \tau$ is the characteristic time governing the equilibrium attainment between secondary electron production and loss rates. $L_y/v = t$ is the transit time of mixture in the discharge chamber. When $\tau \ll t$ the equation (4) reads in the known form:

$$I_s \simeq \frac{e v_{D_0} L_z L_y \beta_0}{2\alpha_0} (R(I_b) - 1) \tag{6}$$

so that:

$$I_b \simeq K_{\alpha_0} I_s^2 + K_{\beta_0} I_s, \tag{7}$$

where

$$K_{\alpha_0} = \frac{\alpha_0}{\varepsilon_0 v_{D_0}^2 e^2 L_z L_y}, \tag{8}$$

$$K_{\beta_0} = \frac{\beta_0}{\varepsilon_0 e v_{D_0}} \tag{9}$$

An inspection of figure 2 shows that we are not dealing with an attachment dominated plasma. In that case, in fact, equation (7) would anticipate a linear dependence on I_s. It turns out that a rather good fit of the experimental data can be obtained using equation (7). By this means one finds at 0·1 atm:

$$\alpha_0 = 5{\cdot}81\ 10^{-7}\ \text{cm}^3\ \text{s}^{-1}, \tag{10}$$

$$\beta_0 = 2{\cdot}76\ 10^{4}\ \text{s}^{-1}, \tag{11}$$

taking $v_{D_0} = 5{\cdot}012\ 10^6\,\mathrm{cm\,s^{-1}}$ as determined in §5, $\varepsilon_0 = 2{\cdot}84 \cdot 10^7\,\mathrm{cm^{-1}\,C^{-1}}$ as given by equation (3) and $L_y L_z = 10 \times 150\,\mathrm{cm^2}$.

It can be verified using values (10 and (11) that $\tau \ll t$ for a typical mixture velocity $v \sim 100$ m/s, so the limiting form (7) of equation (4) is *a posteriori* found to be appropriate to our case. It is worthwhile to note that the values obtained for α_0 and β_0 in such a way are in agreement with data reported by other authors [7, 8]. Since the gas density dependence in equations (4) and (7) has been neglected, the resulting values (10), (11) are to be considered mean values in the discharge channel. However, since $K_{\alpha 0}$ and $K_{\beta 0}$ depend on the numerical values assigned to ε_0 and v_{D0}, the most relevant feature of the procedure is its capability of providing a coherent set of values for α_0, β_0, S_0, v_{D_0}.

3. Kinetic and fluid-dynamic model

The kinetic and fluid-dynamic sets of equations has already been concisely described [1]. One more equation has to be added to take into account the energy stored in the CO vibrational mode:

$$v\frac{d}{dy}E_{CO} = \dot{E}_{CO-e} + \dot{E}_{CO-N_2} + \dot{E}_{CO-v_3}, \tag{12}$$

where $\dot{E}_{CO-x}, x \equiv e, N_2, v_3$ is the production rate of energy in the CO mode due to collisions between CO and electrons, nitrogen and $CO_2(v_3)$ molecules. Analogous terms $\dot{E}_{CO}$, $\dot{E}_{N_2-CO}$ and $\dot{E}_{v_3-CO}$ are to be inserted respectively into the enthalpy, nitrogen and carbon dioxide v_3 mode energy balance equations given in the quoted reference.

As regards the numerical evaluation of the production rate terms $\dot{E}_{x-y}$ we have used the rate-equations approach which has been also described by Douglas-Hamilton and Lowder [7]. Rotational degrees of freedom are supposed to be in Boltzmann equilibrium at the gas temperature T_g. For the rate constants of the $V-V$ and $V-T$ processes involving $CO(v=1)$ data reported by Cheo [9] and Mastrocinque *et al.* [10] have been used. It must be noted here that, though anharmonicity is present in CO, in our calculations harmonic oscillator rules have been generally used to evaluate rate constants for vibrational energy transfers involving higher vibrational levels. For the rate constants of the electron-molecule vibrational excitation of CO the data reported by Thoenes *et al.* [11] as functions of the mean electron energy u_e have been used. In order to evaluate u_e versus the gas density N the curve obtained by Judd [12] for a 3 : 2 : 1 : 0 mixture has been used. As far as we know, in fact, the 6 : 4 : 1 : 1 case is not available in the literature, and it does not seem unreasonable to assume in our case the same electron energy distribution as in the reported case.

Finally, we note here that the source term S as given by equation (3) is proportional to the gas density N. As regards the dependence on N of α and v_D it has been assumed, following Yoder *et al.* [14], that these parameters are proportional to N^2 and $N^{-1/2}$ respectively. The attachment coefficient β has been assumed proportional to N. So we have

$$S(N) = S_0 \cdot N/N_0, \tag{13}$$

$$\alpha(N) = \alpha_0 \cdot N^2/N_0^2, \tag{14}$$

$$\beta(N)=\beta_0 N/N_0, \tag{15}$$

$$\tau_D(N)=\tau_{D_0}(N/N_0)^{1.2}, \tag{16}$$

where N_0 has been set equal to the gas density in the inlet section of the discharge chamber.

4. Small signal gain and optical power calculations

Calculations performed in this section follow in great part those made by Douglas-Hamilton and Lowder [7]. The value of the laser small-signal-gain at the centre of a $P(J_0-1)$ line is equal to:

$$g_0=\left.\frac{\Delta N^{J_0} c^2 g(\nu,\nu_{ba})}{8\pi\nu^2\tau_{ba}}\right|_{\nu=\nu_{ba}} \tag{17}$$

where ΔN^{J_0} is the population difference between roto-vibrational levels $b\equiv(001,J_0)$ and $a\equiv(100,J_0-1)$. τ_{ba} is the radiative lifetime, ν is the laser frequency and $g(\nu,\nu_{ba})$ is the collisionally broadened line shape function centred at ν_{ba}. Its bandwidth $\Delta\nu$ has been calculated using data for collisional cross sections reported by Wood *et al.* [13]. For a CO_2 laser mixture one has:

$$\Delta\nu=10^{-11}NT_g^{1/2}(1{\cdot}2836X_{CO_2}+1{\cdot}2314X_{N_2}+0{\cdot}8705X_{He}+1{\cdot}2315X_{CO}) \tag{18}$$

Using equation (18) for a 6 : 4 : 1 : 1 mixture in equation (17) with $\tau_{ba}=4{\cdot}2$ s and $\nu_{ba}=1/1{\cdot}06\times10^{+3}\,\mathrm{cm}^{-1}$ one gets:

$$g_0=\frac{642{\cdot}13\Delta N^{J_0}}{NT_g^{1/2}}. \tag{19}$$

ΔN^{J_0} is obtained by solving the kinetic set of equations for vibrational populations and using Boltzmann distribution for rotational levels. The rotational quantum number J_0 is generally taken equal to the nearest integer of

$$J_0(\max)=(T_g/1{\cdot}06)^{1/2}, \tag{20}$$

which maximizes the roto-vibrational population inversion. Since in the investigated device the temperature variations experienced by the flowing mixture are not negligible, in our calculations J_0 has been allowed to change continuously along the laser channel and has simply been taken to be given by equation (20).

A fully reliable calculation of the optical output power of the laser requires modelling of the unstable resonator filled with non-uniform gain medium. Such a problem has not been yet studied by us. In order to compare theoretical results with experimental data for the output power and electrical efficiency of the device, a simplified model of the optical cavity, i.e. a Fabry–Perot resonator, has been assumed. The Rigrod equation has been used to calculate the optical energy density flux $\phi_R(y)$ stored in the resonator at the y cross-section:

$$g_c=\frac{g_0(y)}{1+\phi_R(y)/\phi_S(y)}, \tag{21}$$

where g_c, the equivalent cavity loss of the device, has been determined as reported in § 5, and ϕ_S is the saturation flux as given by Douglas-Hamilton and Lowder [7]. The

final equation for the optical power output P_{out} is

$$P_{out} = L_c L_x \int_{y_{min}}^{y_{max}} \frac{g_0(y) - g_c}{2g_c} \phi_s(y) dy, \tag{22}$$

where L_c is the output coupling coefficient of the resonator:

$$L_c = 1 - \frac{\exp(-2L_z g_c)}{1 - M}, \tag{23}$$

M is the effective mirror loss and y_{min}, y_{max} are the initial and final coordinates of the mirrors along the gas flow axis. In fact, as has also been found experimentally, the optimum position of the optical resonator with respect to the discharge chamber is generally dependent both on the kinetic and fluid-dynamic conditions of the device.

5. Numerical results

In this section some results obtained by numerically solving the secondary electron density and the kinetic-and-fluid-dynamic equations for a 6 : 4 : 1 : 1 mixture are reported and discussed. The set of input parameters pertinent to its figures is given in table 2.

Table 2. Input parameters.

P	Initial pressure (atm)	0·1
T_0	Initial temperature (K)	280
α_0	Initial recombination coefficient (cm^3/s)	$5{\cdot}81 \times 10^{-7}$
β_0	Initial attachment coefficient (s^{-1})	$2{\cdot}76 \times 10^{4}$
I_b	Electron beam current (mA)	10–60
U	Electron beam energy after foil (keV)	55
v_{D_0}	Initial electron drift velocity (cm/s)	5×10^{6}
v_0	Initial gas velocity (cm/s)	12×10^{3}
E	Sustainer electric field (V/cm)	333–380
g_c	Cavity gain (cm^{-1})	$0{\cdot}32 \times 10^{-2}$
L_c	Optical output coupling coefficient	0·42
V	Active volume (cm^3)	$10 \times 10 \times 150$

As is shown in figure 3 the numerical results are in agreement with the experimental data for the optical power of the device if one assumes:

$$g_c = 3{\cdot}2 \times 10^{-3}. \tag{24}$$

$$L_c = 0{\cdot}42 \tag{25}$$

$$v_{D_0} = 5{\cdot}0 \times 10^{6} \text{ cm/s}. \tag{26}$$

Theoretical output power values are found to be strongly dependent on g_c, L_c and v_{D_0} so that the determination above is rather accurate. However, it still depends on the assigned values of the initial gas temperature and flow velocity. The value (26) of v_{D_0} is comparable with the 4×10^6 value given by Lowke *et al.* [14] for a 3 : 2 : 1 : 0 mixture and when used in equations (8) and (9) provides a value of α_0 which is very close to those reported in the literature for a 3 : 2 : 1 : 0 mixture. The value of β_0 is sensibly higher than the value theoretically anticipated in a recent paper by Braglia *et al.* [15]. As pointed out by Yoder *et al.* [6] high values of β are probably due to gas impurities.

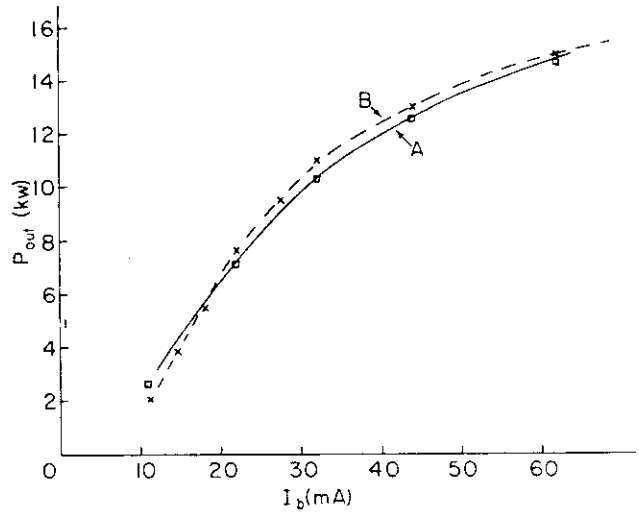

Figure 3. Output power P_{out} versus electron beam current I_b: curve A, numerical; curve B, experimental.

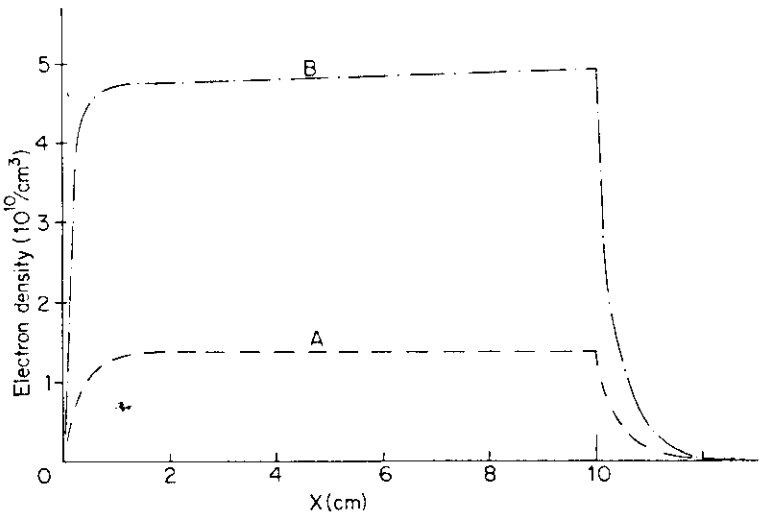

Figure 4. Profiles of secondary electron density N_e along the discharge channel in the gas flow direction: curve A, 59 kW input power; curve B, 190 kW input power.

In figure 4 the space profiles of the secondary electron density in the laser chamber are shown for two values of the input electrical power. The general features of these curves have already been described by Quartieri and Mastrocinque [1]. Here we note that the quasi-stationary value of N_e is practically attained after a distance of about 1 cm. This distance is of the order of $v\tau$, where $\tau = (\beta R)^{-1}$ is the time constant governing the attainment of equilibrium between gas ionization and recombination-and-attachment processes. As the gas flows through the chamber, the equilibrium value of the electron density exhibits a further slow increase due to the variation on

the gas density N in this region. Note in fact that the steady-state value is practically given by

$$N_e \simeq \frac{\beta}{2\alpha}(R-1) \propto \frac{1}{N}\left[\sqrt{\left(\frac{1+4\alpha_0 S_0 N}{\beta_0^2 N_0}-1\right)}\right] \tag{27}$$

where the dependences on N of the various parameters have been taken into account as stated in § 3. Since the overall variation of the gas density in the laser chamber is smaller than 20 per cent, as is shown in figures 5, and 6, a similarly small variation of N_e is found via equation (27). However, the dependence on N of β seems to be in many cases much stronger than that here assumed, so that less uniform electron density and sustainer current profiles could be possible in the real system.

Figure 5 and 6 show velocity, temperature and density profiles of the fluid in the laser chamber for two values of the input electrical power. We note, for instance, that the temperature increase is about 12 and 40 K in the two cases respectively. The temperature increase in the after-discharge region is due to V–T energy relaxation. Both the direct gas heating due to electron–molecule collisions and indirect power injection in the translational degree of freedom from the vibrational ones are found to be important. Since the direct gas heating depends strictly on the electrical power density, it can be thought that the dependence on N of β can produce relevant effects on the space profiles of all the fluid-dynamic parameters.

In figure 7 two small signal-gain profiles are shown for two values of the input electrical power. These profiles appear rather asymmetric with respect to the centre of the discharge chamber, so that optimum output coupling requires a displacement of the optical resonator position in the flow direction. We have assumed the Fabry–Perot cavity ($10 \times 10 \times 150\,cm^3$ active volume) centred at 8·0 cm from the inlet cross section. The maximum value of the curves is attained at the exit cross section, so that operation with a lower gas flow velocity would provide a greater efficiency. However, in a real system, when the mixture transit time in the laser chamber is too long, discharge instabilities can arise.

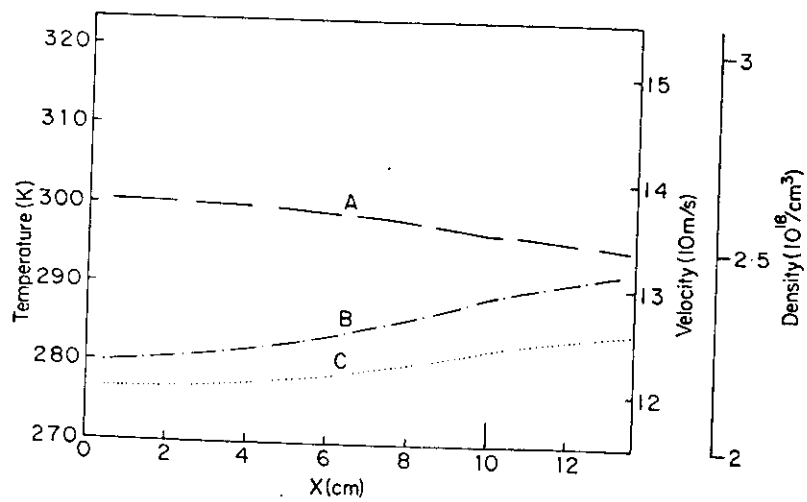

Figure 5. Profiles of some thermo-fluid-dynamic parameters along the discharge channel in the gas flow direction in the case of 59 kW input power: curve A, density, curve B, temperature; curve C, velocity.

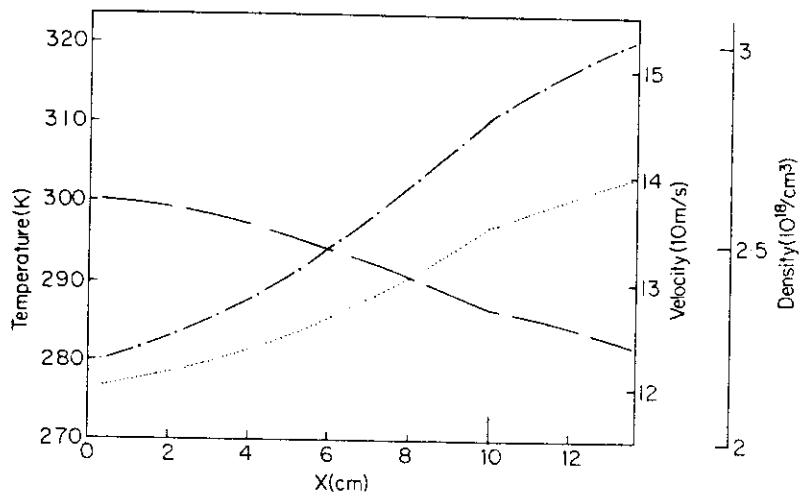

Figure 6. Profiles of some thermo-fluid-dynamic parameters along the discharge channel in the gas flow direction in the case of 190 kW input power: curve A, density; curve B, temperature; curve C, velocity.

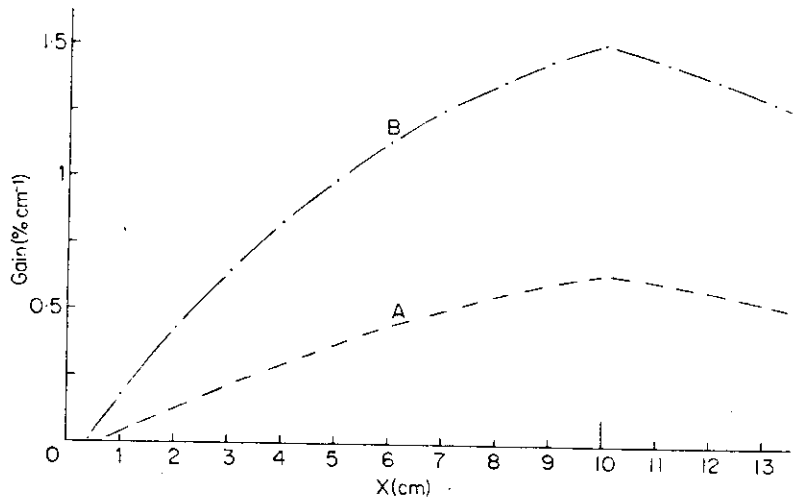

Figure 7. Small-signal-gain profiles along the discharge chamber in the gas flow direction: curve A, 59 kW input power; curve B, 190 kW input power.

In figure 8 two saturation-flux profiles are shown for the two investigated cases. The main feature of these curves is that temperature increments in the laser channel produce a relevant increase of ϕ_S. This fact is to be taken into account when studying optical beam inhomogeneities.

6. Conclusions

The main features of a c.w. high power CO_2 laser model have been outlined and some numerical results have been presented. So far no account has been taken of the effects produced on the gas mixture kinetics by chemical reactions, dissociation or laser radiation. The dependence on the gas density of various plasma parameters has been assessed on the basis of statements reported in the literature, and the optical

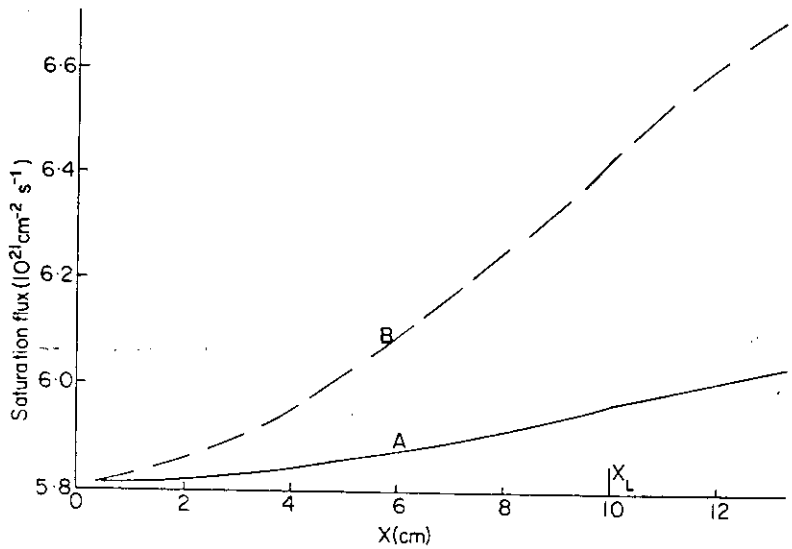

Figure 8. Saturation flux profiles along the discharge channel in the gas flow direction: curve A, 59 kW input power; curve B, 190 kW input power.

cavity model is a simplified one. However, rather good fits of some experimental data have been obtained, and the resulting values for uncertain parameters seem to form a coherent and reasonable set. Thus the model seems adequate to provide a check on some unknown effects, such as electrical excitation inhomogeneities, vibrational anharmonicity, mixture composition variations etc. If coupled with a more adequate optical cavity model, it could be useful in investigating optical beam inhomogeneities produced by density and temperature effects.

Acknowledgments

We are indebted to the U.R. Fisica of the Centro Ricerche Fiat, Orbassano (TO), Italy, for providing experimental data.

Nous avons étudié quelques problèmes de cinétique, de dynamique des fluides et d'électricité qui se présentent dans la modélisation numérique d'un laser continue TE haute puissance à CO_2 fonctionnant dans un mélange contenant N_2, H_2 et CO. Nous avons adapté un modèle à cinq températures d'un laser impulsionnel au cas d'un laser continu en couplant un système d'équations de dynamique des fluides à celui de cinétique. Nous avons ajouté l'équation donnant la proportion d'électrons secondaires. Nous avons calculé en détail le terme d'ionisation et tenu compte des résultats expérimentaux pour déterminer les coefficients d'attachement et de recombinaison. Un code numérique a été développé pour résoudre nos équations. Par ce moyen, nous avons examiné les effets de la température, de la densité et des variations de vitesse dans le mélange en écoulement sur le faible gain de signal du système. Nous avons obtenu des profils dans la cavité laser du courant de soutien, du faible gain de signal et des paramètres de dynamique des fluides. Un modèle de cavité optique simple (Fabry–Perot) a été utilisé pour calculer la puissance de sortie et l'efficacité électrique du système. Une comparaison des prédictions du code numérique et des résultats expérimentaux est présentée.

References

[1] Quartieri, J., and Mastrocinque, G., 1979, *Lett. nuovo Cim.*, **25**, 328.
[2] Rohrlich, F., and Carlson, B. C., 1954, *Phys. Rev.*, **93**, 38.

[3] BIRKHOFF, R. D., 1950, *Handbuch der Physik*, Vol. 34 (Berlin, Heidelberg, New York: Springer-Verlag).
[4] BERGER, M. J., and SELTZER, S. M., 1964, *Tables of energy losses and ranges of electrons and positrons*, NASA SP-3012, p. 127.
[5] MARTELLUCCI, S., QUARTIERI, J., MASTROCINQUE, G., and SOLIMENO, S., 1979, *Nuovo Cim.* B, **54**, 99.
[6] YODER, M. J., LEGNER, H. H., JACOB, J. H., and AHOUSE, D. R., 1978, *J. appl. Phys.*, **49**, 5073.
[7] DOUGLAS-HAMILTON, D. H., and LOWDER, R. S., 1974, *AERL Kinetics Handbook*, AVCO Report N. AFWL TR-64-216, p. 194.
[8] CENTER, R. E., 1973, *J. appl. Phys.*, **44**, 3528.
[9] CHEO, P. K., 1974, *Lasers* (New York: Levine and De Maria).
[10] MASTROCINQUE, G., DOYENNETTE, L., CHAKROUN, A., GUEGUEN, H., MARGOTTIN-MACLOU, M., and HENRY, L., 1976, *Chem. Phys. Lett.*, **39**, 347.
[11] THOENES, J., KURZIUS, S. C., and PEARSON, M. L., 1975, Lockheed Technical Report RG-CR-75-2.
[12] JUDD, O., 1975, *High-Power Gas Lasers, Inst. Phys. Conf. Ser. No* 29, edited by R. E. Pike (London, Bristol: The Institute of Physics), p. 37.
[13] WOOD, A. D., *et al.*, 1968, *High Power Laser Techniques*, Vol. II, AFAL-TR-68-361.
[14] LOWKE, J. J., PHELPS, A. V., and IRWIN, B. W., 1973, *J. appl. Phys.*, **44**, 4664.
[15] BRAGLIA, G. L., BRUZZESE, R., and CARAFFINI, G. L., 1979, *Lett. nuovo Cim.*, **25**, 139.